Engineering Solid Mechanics 7 (2019) 367-381

Contents lists available at GrowingScience

Engineering Solid Mechanics

homepage: www.GrowingScience.com/esm

The effects of adding silicon carbide SiCp on aluminum alloy and analyzing the fatigue parameters and mechanical properties for metal matrix composites

Dr Mazin Mahmood Yahya[a*]

[a]*Aeronautical Techniques Engineering Department (Head of Department), Bilad Alrafidain University College, Iraq*

ARTICLE INFO

Article history:
Received 2 June, 2018
Accepted 7 July 2019
Available online
7 July 2019

Keywords:
Low Cycle Fatigue Parameters
Metal Matrix Materials
Cyclic stress-Cyclic Strain Life
SEM of MMCs
Transition Life of MMCs

ABSTRACT

The low cycle fatigue (LCF) resistance of two different metal matrix composite (MMC) of AA6063 with 2% and 8% by volume silicon carbide (SiCp) particles having particulate size of 37 micron (400 mesh) at room temperature condition has been evaluated under fully reversed strain control testing. The influence of volume fraction (2 and 8 vol%) and strain ratio (R= -1) are examined. Increasing the content of SiCp results in the degradation of strain control fatigue properties while the transition fatigue life increases. Fatigued samples are examined using scanning electron microscopy in order to understand the failure mechanism (SEM). Microstructural features and failure mechanisms studied through scanning electron microscopy (SEM) confirmed low cycle fatigue failure nature.

1. Introduction

Metal matrix composites (MMCs) are promising materials for lightweight, high strength structural applications, in particulate MMCs non-metallic particles are incorporated in metallic alloys to improve their elastic modulus and strength, introducing reinforcement particles with high modulus to the matrix alloy can reduce the fracture toughness and change the fatigue resistance of the material. The effects of reinforcement on cyclic fatigue damage and crack initiation, its role on constraining matrix plastic flow during cyclic deformation and the response of the material are important aspects in low cycle fatigue (LCF) of MMCs.

Al-Si cast alloy reinforced by SiC-particulate with two different volume fractions has been investigated by Koh et al. (1999) under strain-controlled conditions with and without tensile mean strains. The composites and the unreinforced matrix alloy showed cyclic hardening behaviour. The initial high tensile mean stress relaxed to zero for the ductile Al-Si alloy. Hall et al. (1994) has reported the strain-controlled low-cycle fatigue (LCF) behaviour of AA2124 aluminum alloy SiCp MMC. Ding et al. (2002) reported low cycle fatigue behavior of AA6061 aluminum alloy reinforced with Al_2O_3 particles in two volume fractions of 15% and 20%. The results obtained from theoretical model was verified with that obtained experimentally using total strain-controlled symmetrical push-pull fatigue tests.

* Corresponding author.
E-mail addresses: mmyahya.rs.mec11@iitbhu.ac.in (M.M. Yahya)

doi: 10.5267/j.esm.2019.7.001

The effect of SiC volume fraction and particle size on the fatigue behavior of AA2080 alloy was investigated by Chawla et al. (1998). Increasing volume fraction and decreasing particle size resulted in an increase in fatigue resistance. The effect of inclusion size and location on fatigue life of the composites is discussed. Hadianfard and Mai (2000) studied the low cycle fatigue (LCF) resistance of two different AA6061 alloy reinforced with 20 vol% alumina particulate metal matrix composite. Both MMCs exhibit short LCF life which follows a Coffin-Manson relationship. All tested specimens demonstrate ductile fracture morphology at final failure. The experimental results are discussed in respect of strain amplitude, matrix composition and reinforcement shape and crack initiation. Shang and Ritchie (1989) studied micro-mechanisms of crack-tip shielding associated with the growth of fatigue cracks in metal-matrix composites with specific emphasis on the role of un-cracked ligaments. The predicted degree of shielding derived from these mechanisms is not large, but is found to be consistent with experimental observations in high-strength aluminum alloys reinforced with 15 to 20 vol % of SiC particles. Muratoglu et al. (2006) investigated the SiC particulate reinforced aluminum metal matrix composites (MMCs) with pure aluminum by diffusion bonding process. The application of aging before and after diffusion bonding decreases SiC particulate accumulation (Srivatsan, 2002).

Uygur and Kulekcl (2002) used powder metallurgy processed metal matrix composites and performed fatigue testing under the strain control loading conditions. The influence of volume fraction (17 and 25 vol%), particulate size (2.5 and 15 μm) of reinforcement particles and strain ratio (R=0, R=0.5 and R= -1) are examined for AA2124+SiCp composite under T4 condition. The monotonic and cyclic stress-strain response was significantly altered by strain ratio values. Li et al. (2010) studied low-cycle fatigue life and cyclic stress response of SiCp/Al–Si composites produced by spray deposition in comparison to the unreinforced alloy. Both the composite and matrix alloy display cyclic hardening under total-strain amplitude of 0.35–0.5%. Under low strain amplitude (0.3%), the Al–Si alloy shows cyclic. In this research low cycle fatigue resistance of two different MMCs of AA6063 with 2% and 8% by volume silicon carbide (SiCp) particles is evaluated under fully reversed strain control testing and at room temperature condition.

2. Methodology

2.1 Chemical Composition Test

Chemical composition test is performed using “Thermo Scientific ARL Optim: X-Ray Analyzer 166”as shown in Fig. 1, with supply voltage 230V-1.5 KV to understand the chemical composition of the specimen.

2.2 EDAX-SEM Test

Chemical composition is also studied through EDAX analysis. The quantitative analysis by EDAX is performed with a relatively high voltage of 10 KV to improve the contrast between metallic and matrix phases. Microstructural features and failure mechanisms are studied through scanning electron microscopy (SEM). The SEM-EDAX system used is FEG Quanta -200 as shown in Fig. 2.

Fig. 1 X-RF Analyzer 166 Machine

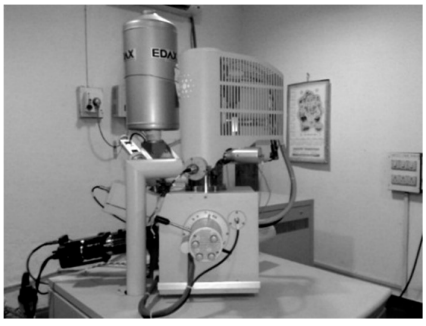

Fig. 2 SEM and EDAX machine

2.3 Tensile Test

Before fatigue test, the monotonic tensile test is performed with cylindrical Hounsfield tensile specimen with gauge length, 15.4 mm and gauge diameter 4.5 mm as shown in Fig. 3, at a nominal strain rate of 1.2×10^{-4} s^{-1} using Instron 4206 machine having loading capacity of 100kN as shown in Fig. 4, using test methods specified by ASTM Standards E8 and E606 (2005).

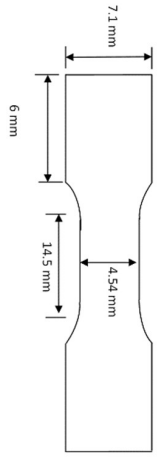

Fig. 3 Tensile test specimen

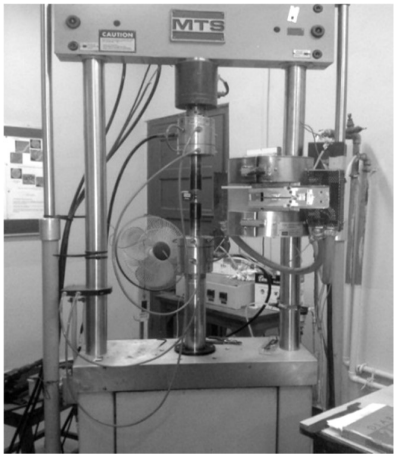

Fig. 4 Tensile Testing Machine

2.4 Torsion Test

Torsion test is also performed with the sample as shown in Fig. 5 using Torsion testing machine of Avery (7601 CHG), Birmingham, England having capacity 60000 kg.cm as shown in Fig. 6.

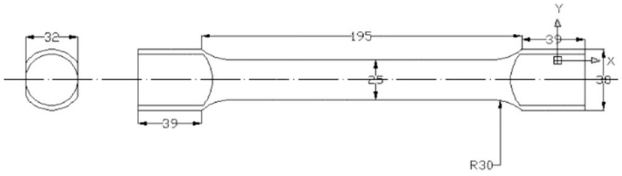

Fig. 5 Torsion test specimen

Fig. 6 Torsion testing machine

2.5 Fatigue Test

Cantilever Beam Specimen

Figure 7 shows the geometry of the cantilever specimen for rotating low cycle fatigue test with gage length 106 mm and gage diameter 8 mm. The test is done using WP 140 Fatigue Testing Apparatus, Gunt, Hamburg, Germany as shown in Fig.8.

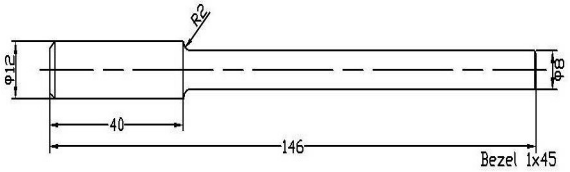

Fig. 7 Cantilever fatigue test specimen

Fig. 8 Cantilever fatigue machine

2.6 X-RD Test

X-ray Diffraction tests were performed using Rigaku-Mini Flex II Desktop-X-Ray Diffractometer as shown in Fig. 9.

2.7 Optical Micrograph Test

Optical micrography is studied for fatigue test samples using metallux-3 optical microscope of Carl Zeiss Micro Imagine Gmb H 37081, Germany as shown in Fig.10. The samples are prepared by etching with a solution containing HNO_3, HF and water in proportion of 5% , 10% and 85%, respectively by volume .

Fig. 9 X-Ray diffract meter test setup

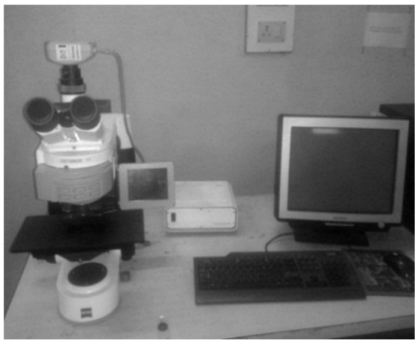

Fig. 10 Optical micrograph test setup

2.8 Hardness Test

Micro hardness test is carried out using HMV-2 shimadzu micro hardness tester as shown in Fig. 11, of the AA 6063 alloy subjected to the different applied load.

Fig. 11 Micro hardness test setup

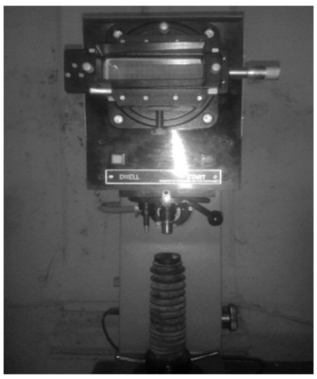

Fig. 12 Vickers macro hardness (HV) machine

Vickers micro hardness (HV) is measured on the plane surface with different loads. Prior to each hardness measurement, the surfaces of the specimen is polished mechanically using emery paper and alumina liquid to remove the surface reactions.

An average of at least three readings on the surface of the specimen are taken to obtain a micro hardness value. Vickers macro hardness (HV) test was done with different applied load using Vickers Macro Hardness testing machine of model MECH C.S/VM50, as shown in Fig. 12.

Sample of main text. Sample of main text. Sample of main text. Sample of main text. Sample of main text. Sample of main text. Sample of main text. Sample of main text. Sample of main text. Sample of main text. Sample of main text.

3. Ansys Analysis

The ANSYS program has many finite element analysis capabilities ranging from a simple, linear, static analysis to complex, non linear, transit dynamic analysis. The process for a typical ANSYS analysis involves in three general tasks: Building the model, Appling the loads and obtaining the solution and Reviewing the results.

The current problem of rotating cantilever low cycle fatigue analysis is modeled as a static problem by introducing centrifugal forces arising from the rotation and applying the time varying bending force at the free end. Boundary conditions are shown in Fig. 13. The element used for the present analysis is PLANE182 available in Ansys software which is a two dimensional four nodded structural solid element. PLANE182 is used for 2-D modeling of solid structures. The element can be used as either a plane element (plane stress, plane strain or generalized plane strain) or an axisymmetric element. It is defined by four nodes having two degrees of freedom at each node: translations in the nodal x and y directions. The element has plasticity, hyperelasticity, stress stiffening, large deflection, and large strain capabilities. It also has mixed formulation capability for simulating deformations of nearly incompressible elastoplastic materials, and fully incompressible hyperelastic materials.

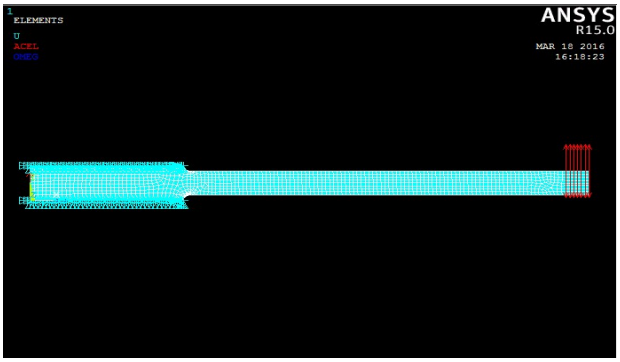

Fig. 13 Meshed model of cantilever beam with boundary conditions

4. Theoretical analysis

4.1 Tensile Analysis

The strain hardness exponent (n) and strength coefficient (K) can be obtained from log-log plot of true plastic stress and true plastic strain. The slope of the plot gives (n) and intercept of the plot at unit plastic strain gives (K) based on the relation (Knez et al., 2010):

$$\sigma = K\varepsilon_p^n \tag{1}$$

4.2 Low Cycle Fatigue (LCF) Analysis

The theoretical investigation of low cycle fatigue (LCF) is performed using the method elaborated by Eleiche et al. (1996). The adopted process for the present analysis is described as follows. According to Basquin, the strain-life data can be linearized on log-log scale as:

$$\frac{\Delta\varepsilon_e}{2} = \frac{\sigma_f'}{E}\left(2N_f\right)^b \tag{2}$$

Coffin and Manson found that the plastic strain-life data could also be linearized on log–log scale as:

$$\frac{\Delta\varepsilon_p}{2} = \varepsilon_f'\left(2N_f\right)^c \tag{3}$$

The total strain amplitude can then be considered as the summation of elastic and plastic amplitudes and the resulting strain-life curve can be expressed as:

$$\varepsilon_a = \frac{\Delta\varepsilon_e}{2} + \frac{\Delta\varepsilon_p}{2} = \frac{\sigma_f'}{E}\left(2N_f\right)^b + \varepsilon_f'\left(2N_f\right)^c \tag{4}$$

Where σ_f' is the fatigue strength coefficient, b is the fatigue strength exponent, ε_f' is the fatigue ductility coefficient and c is the fatigue ductility exponent. The life at which elastic and plastic components of strain are equal is called the transition fatigue life (2Nt). For lives shorter than 2Nt the deformation is mainly plastic, whereas for lives longer than 2Nt the deformation is mainly elastic. The cyclic strength coefficient, K′, and the cyclic strain hardening exponent, n′ can be estimated from the low-cycle fatigue parameters as follows:

$$\mathrm{K}' = \frac{\sigma_f'}{\left(\varepsilon_f'\right)^{\frac{b}{c}}} \tag{5}$$

$$\mathrm{n}' = \frac{b}{c} \tag{6}$$

5. Results

5.1 Tensile Data

Tensile tests were carried out at room temperature. Tensile engineering stress-strain curves of the as received AA6063 alloy is shown in Fig. 14, and for the metal matrix composite of AA6063 with 2% and 8% SiCp are shown in Fig. 15 and Fig. 16, respectively. The tensile test parameters for these cases are shown in Table 1.

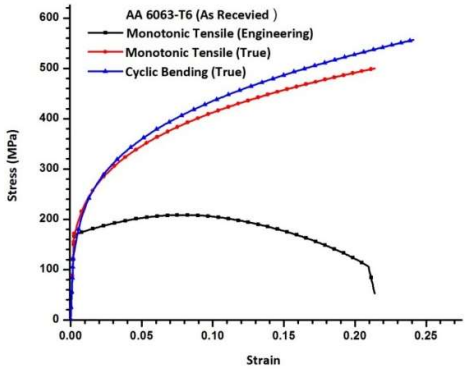

Fig. 14 Stress - Strain Curves for AA6063-T6 received

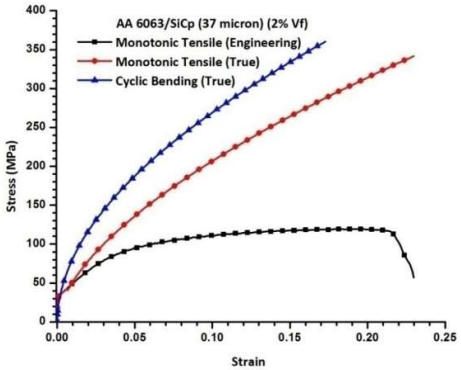

Fig. 15 Stress-strain curves for alloy as AA6063+SiCp (37 micron, 2V_f%)

True plastic stress versus true plastic strain is plotted in log-log scale for the samples as shown in Fig. 17 and n, k values are calculated for all cases and presented in Table 1.

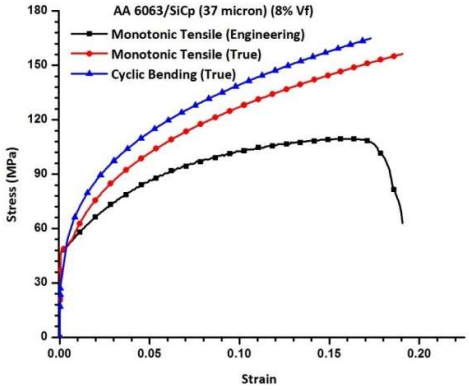

Fig. 16 Stress-strain curves for AA6063+SiCp (37 micron, 8V_f%)

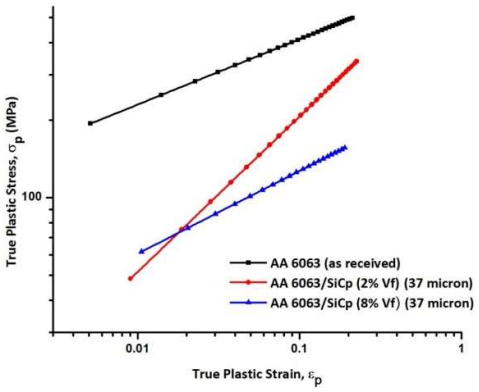

Fig. 17 Log-Log true plastic stress versus true plastic strain plot with different volume fraction of SiC reinforcement particle

Table 1 The monotonic propretés of AA6063 at different volume fraction of SiC reinforcement particle

Conditions	**n**	σ_f	**K**	$\sigma_{fracture}^{true}$	σ_y **(MPa)**	σ_{Max} **(MPa)**	$\varepsilon_{Frac.}$	**E (GPa)**
As Received	0.25	859.5	776.2	237.49	169.67	192.76	0.2745	68
AA6063+SiCp (2% V_f)	0.492	534.4	829.8	85.164	42.6167	118.9	0.274	72
AA6063+SiCp (8% V_f)	0.285	188.34	266.07	85.046	52.8471	126.8	0.235	75

Figure 18 shows the cyclic true bending stress-strain plots for as-received and two categories of MMCs considered in the study.

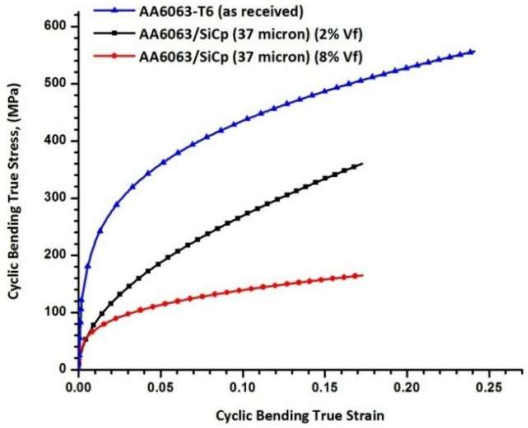

Fig. 18 Cyclic Bending True Stress-Strain Curves of AA6063+ SiCp with different volume fraction of reinforcement particle

5.2 Fatigue Data

Cyclic data have been collected from the cantilever fatigue test for MMC sample having composition AA 6063 with 2% by volume SiC particles at room temperature condition. The strain-life relation is plotted for this said sample and shown in Fig 19. The plot illustrates elastic strain line, plastic strain line and total strain curve. The plot also shows transition fatigue life and two region viz. elastic

and plastic region. In a similar way, the low cycle fatigue data for other MMC sample i.e. AA6063-8% by volume of SiC particle. The strain-life relation for this case is illustrated in Fig 20.

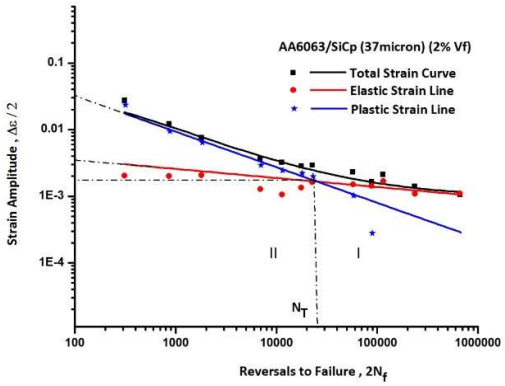

Fig. 19 Strain life curves for AA6063+ SiCp (2% V_f)

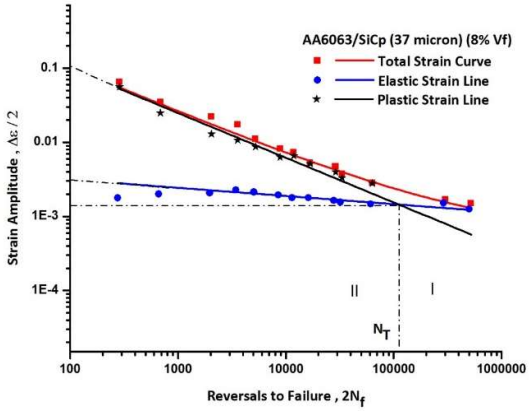

Fig. 20 Strain life curves for AA6063+ SiCp (8% V_f)

The comparison of different fatigue parameters viz. $\boldsymbol{\varepsilon_f'}$, $\boldsymbol{\sigma_f'/E}$, ***b, c,*** **n′, K′** and $\mathbf{N_T}$ are shown in Table 2 for two MMC cases and as received case.

Table 2 Low cycle fatigue properties of aluminum alloy AA6063+ SiCp with different volume fraction V_f % of reinforcement particle size

Alloy	Cyclic plastic strain ε_f'	Cyclic elastic strain σ_f'/E	Fatigue Strength Coefficient σ_f' (MPa)	fatigue strength exponent b	fatigue ductility exponent c	cyclic strain hardening exponent n′	cyclic strength coefficient K′ (MPa)	transition fatigue life N_T (cycles)
As received 6063-T6	0.69	0.0086	586.16	-0.105	-0.72	0.14583	618.75	2170
6063/SiC (2% Vf)	0.0488	0.0086	622.8	-0.079	-0.47	0.1680	1034.27	25621
6063/SiC (8% Vf)	0.476	0.0077	583.5	-0.094	-0.59	0.159	656.6	107721

Figure 21 elaborates total strain-life curves for as received AA6063, AA6063/ 2volume 2% SiCp MMC and AA6063/ 8volume % SiCp for two low cycle fatigue test. The comparison shows that MMC with 8 volume % SiCp is having maximum transition fatigue life. Fig. 22 illustrates variation of transition fatigue life with the respect to volume % of SiCp in MMC and it is observed that the transition fatigue life increases with volume % of SiCp.

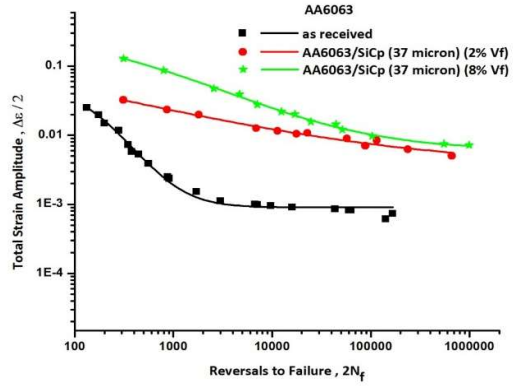

Fig. 21 Total strain-life curves for AA6063+SiCp with different reinforcement volume fraction SiCp

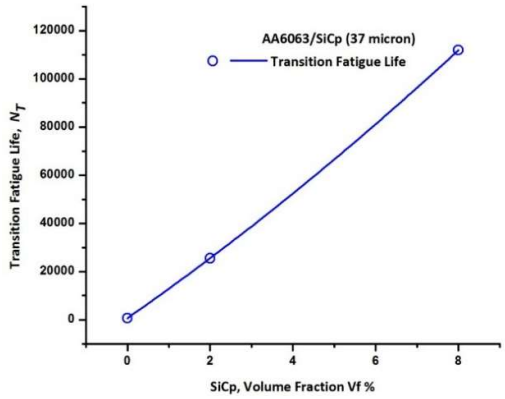

Fig. 22 Transition life variation with different volume fraction V_f % of particle SiCp size

5.3 XRD Data

Figure 23 and 24 shows XRD patterns for AA6063/SiCp (2% V_f) MMC and AA6063/SiCp (8% V_f) MMCs, respectively at room temperature condition. Table 3 shows data of crystallite size, diameter of sample at fracture and numbers of cycles of failure for as received AA6063, AA6063/SiCp (2% V_f) MMC and AA6063/SiCp (8% V_f) MMCs. The variation of crystallite size with different volume fraction of reinforcement particle of MMC illustrate in Fig. 25. It is observed that the crystallite size has a increase till certain volume fraction after that decrease. And the variation of crystallite size with different volume fraction of reinforcement particle of MMC. Also it is observed that the crystallite size has a increase till certain volume fraction after that decrease.

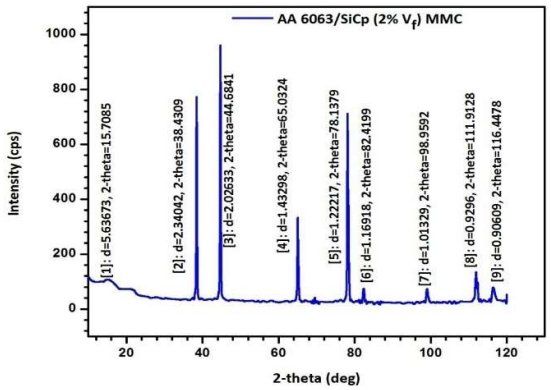

Fig. 23 X-RD pattern for AA6063/SiCp (2% V_f) MMC

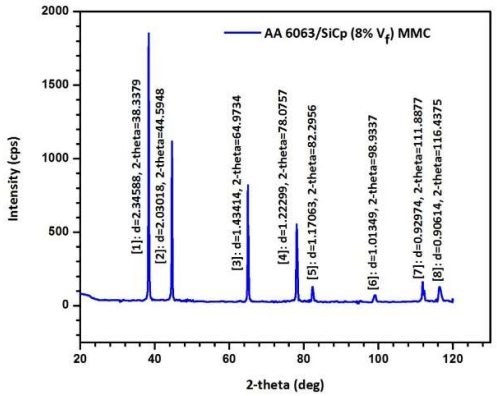

Fig. 24 X-RD pattern for AA6063/SiCp (8% V_f) MMC

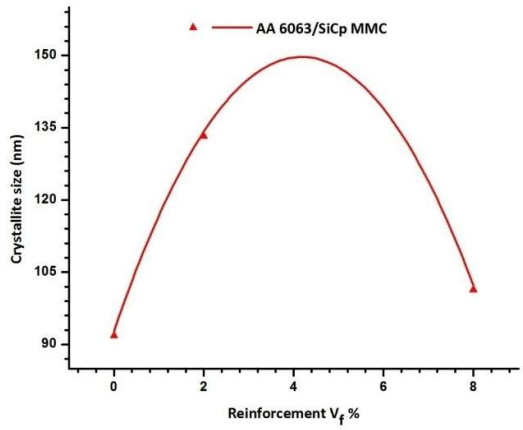

Fig. 25 Variation of crystallite size with different volume reinforcement particle of AA6063/SiCp V_f MMC

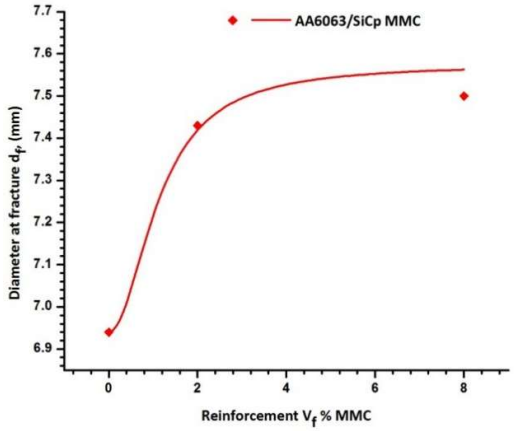

Fig. 26 Variation of diameter at fracture of sample with different fraction of reinforcement particle of MMC

Figure 26 illustrates variation of crystallite size with reinforcement volume fraction of MMC. The variation of diameter of sample at fracture with reinforcement volume fraction of MMC is demonstrated in Fig. 27. It is observed that the diameter of sample at fracture has a decreasing tendency with number of cycles to failure.

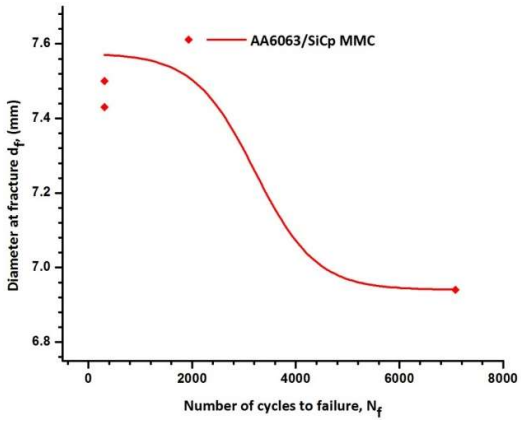

Fig. 27 Variation of diameter of sample at fracture with the number of cycles to failure of reinforcement particle of MMC

Table 3 shows data of crystallite size, diameter of sample at fracture and numbers of cycles of failure for as received AA6063, AA6063/SiCp (2% V_f) MMC and AA6063/SiCp (8% V_f) MMCs.

Table 3 Crystallite size and diameter of sample at fracture data for AA6063/SiCp MMC

Samples	Crystallite size nm	Diameter of sample at fracture (mm)	Number of cycles of failure, N_f
As received AA6063	91.834	6.94	7080
AA6063/SiCp (2% V_f)	133.26	7.43	311
AA6063/SiCp (8% V_f)	101.37	7.5	310

5.4 FEM Result

It is also observed from Table 4 and Table 5 that Prediction for elastic and plastic strain by Morrows method is very good.

Table 4 Comparison of experimental, numerical results for elastic strain AA6063 for Metal Matrix Composite at different volume fraction of SiCp reinforcement particle

Condition	Force (N)	Cycles	Elastic Strain				
			Exp.	FEM	% Diff.	Morrow	% Diff.
6063/SiCp 37 micron (2%Vf)	65	311	0.00191	0.001904	0.298	0.005497	65.25
6063/SiCp 37 micron (8%Vf)	57	310	0.00162	0.001750	8.03	0.004537	64.29

Table 5 Comparison of experimental, numerical results for Plastic strain AA6063 for Metal Matrix Composite at different volume fraction of SiCp reinforcement particle

Condition	Force (N)	Cycles	Plastic Strain				
			Exp.	FEM	% Diff.	Morrow	% Diff.
6063/SiCp 37 micron (2%Vf)	65	311	0.02555	0.025834	1.11	0.00329	87.134
6063/SiCp 37 micron (8%Vf)	57	310	0.06186	0.063676	2.9	0.016133	73.921

Figure 28 and Fig. 29 illustrate variation of elastic and plastic strains over time at a particular node on the surface of the specimen along the fracture cross-section. It is observed from the figure that plastic strain is constant over time while elastic strain varies between maximum value of 0.00196123 and

minimum value of 0.00138948 for AA6063/SiCp (2% V_f) MMC and maximum value of 0.00175016 and minimum value of 0.00131551 for AA6063/SiCp (8% V_f) MMC.

Figures 30 and 31 show deformed shape of the specimen of AA6063/SiCp of (2% V_f) MMC at a particular instant of time with elastic and plastic strain distributions, respectively. Figures 32 and 33 show deformed shape of the specimen of AA6063/SiCp (8% V_f) MMC at a particular instant of time with elastic and plastic strain distributions, respectively.

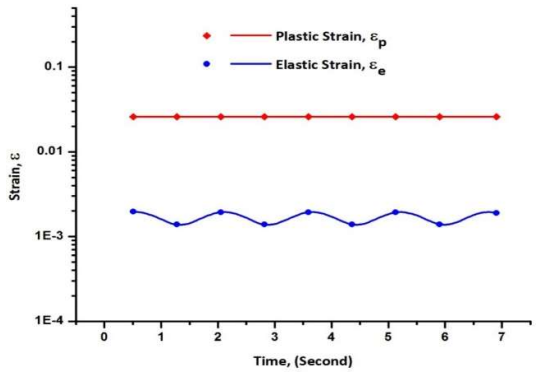

Fig. 28 Time history plot of elastic and plastic strain at surface node on cross section of fracture for AA6063/SiCp (2% V_f) MMC

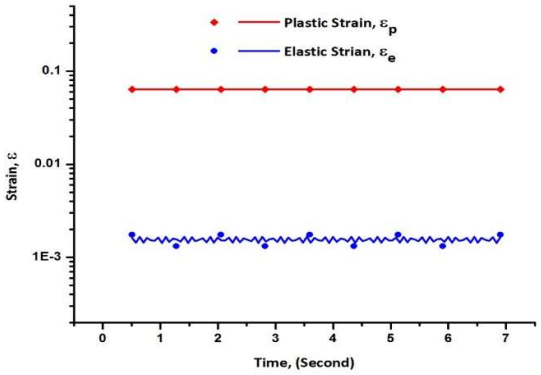

Fig. 29 Time history plot of elastic and plastic strain at surface node on cross section of fracture for AA6063/SiCp (8% V_f) MMC

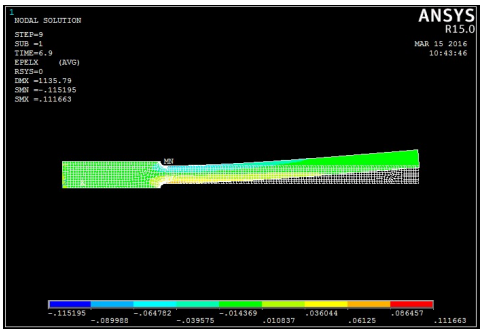

Fig. 30 Elastic strain at particular time on deformed shape for AA6063/SiCp of(2%V_f) MMC

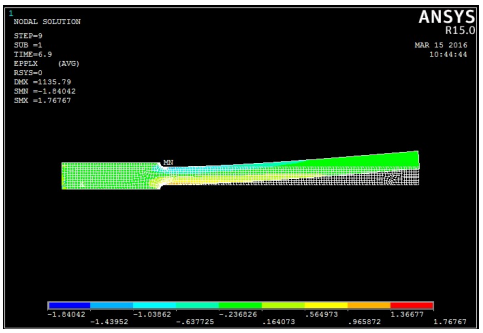

Fig. 31 Plastic strain at particular time on deformed shape for AA6063/SiCp(2% V_f) MMC

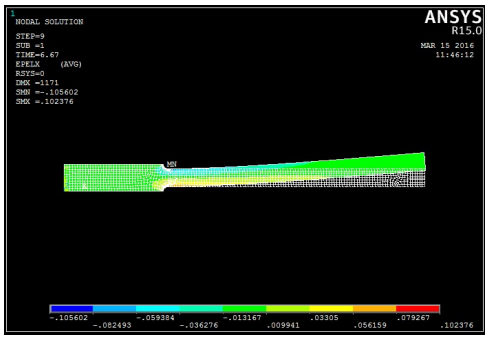

Fig. 32 Elastic strain at particular time on deformed shape for AA6063/SiCp (8% V_f) MMC

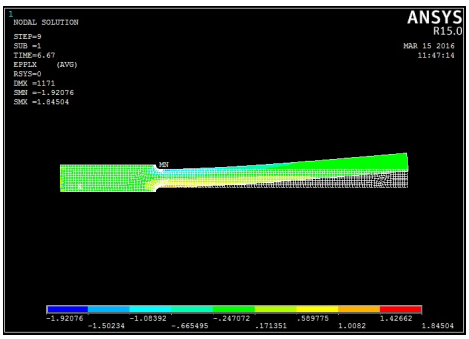

Fig. 33 Plastic strain at particular time on deformed shape for AA6063/SiCp (8% V_f) MMC

5.5 Microstructure Data

Figure 34 shows optical micrograph pictures of AA6063/SiCp MMC for 2% V_f and 8% V_f cases at 50x,100x and 200x magnification before LCF test. The micrographs clearly show the SiCp particales and more densities are observed for 8% V_f MMC than 2% V_f MMC.

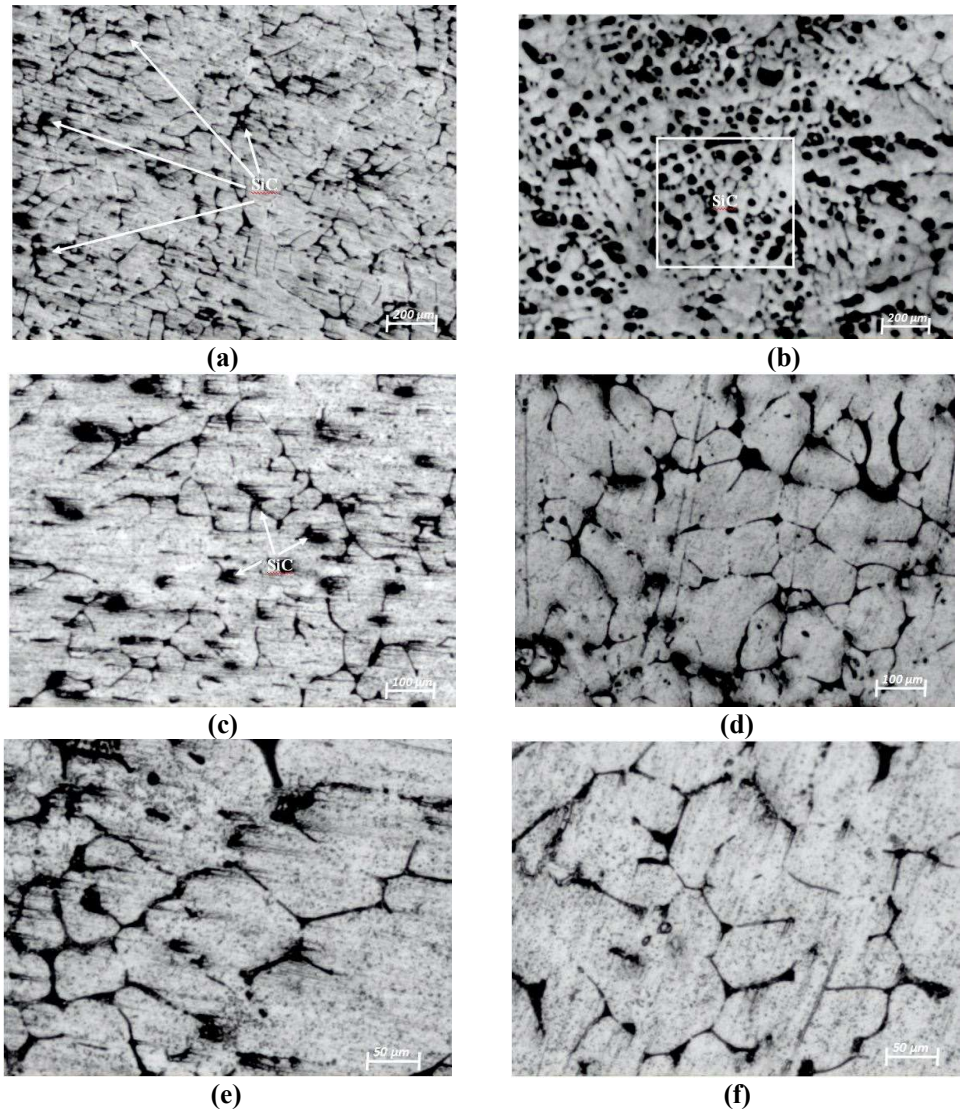

Fig. 34 Microstructure of the AA6063/SiCp MMC: (a) 2% V_f 50x magnification, (b) 8% V_f 50x magnification, (c) 2% V_f 100x magnification, (d) 8% V_f 100x magnification (e) 2% V_f 200x magnification, (f) 8% V_f 200x magnification

5.6 SEM Data

The fracture surfaces of the specimens after fatigue testing were examined using scanning electron microscope. Fatigued specimens at different volume fraction were selected in order to study the characteristics of the fatigue crack formation and growth.

All fracture surfaces had a dimple morphology, which indicates ductile fracture mode. Most of these dimples resulted from fracture or decohesion of SiC particles. There were mainly two dimple populations: the first one was related to SiC particles and increased in size as the size of the reinforcement particles were increased. The second population consisted of very small dimples located in the space between the reinforcement particles associated with fine intermetallic particles as observed in Fig. 35.

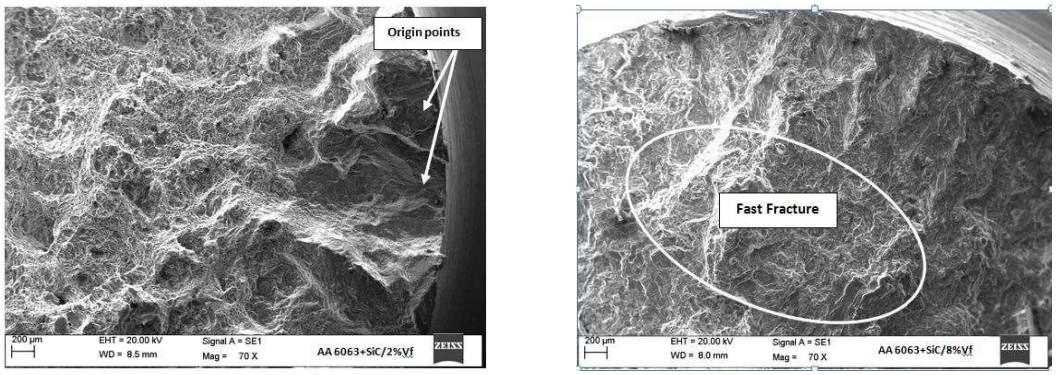

(a) **(b)**

Fig. 35 SEM micrographs over view from the edge fracture surface of MMC AA6063/SiCp with (a) 2% V_f, (b) 8% V_f

The particle cracking and cleavage between SiC and matrix material became more evident as the SiC size and content increased. There were a few observations of pull out of particles from the aluminium matrix, which indicates quite a good interfacial bonding as shown in Fig.35. High magnification SEM picture shows particle cracking and cleavage between SiC particle and matrix material on fracture surface as shown in Fig. 36.

Two distinct fracture morphologies were observed: an initiation region and a fast fracture region. Higher magnifications of these two regions show that the fracture region around the initiation site did not have as many fractured or decohered particles as can be observed in Figs. 36 (a, b) and the fast fracture region can be observed from Figs. 36 (c, d) .

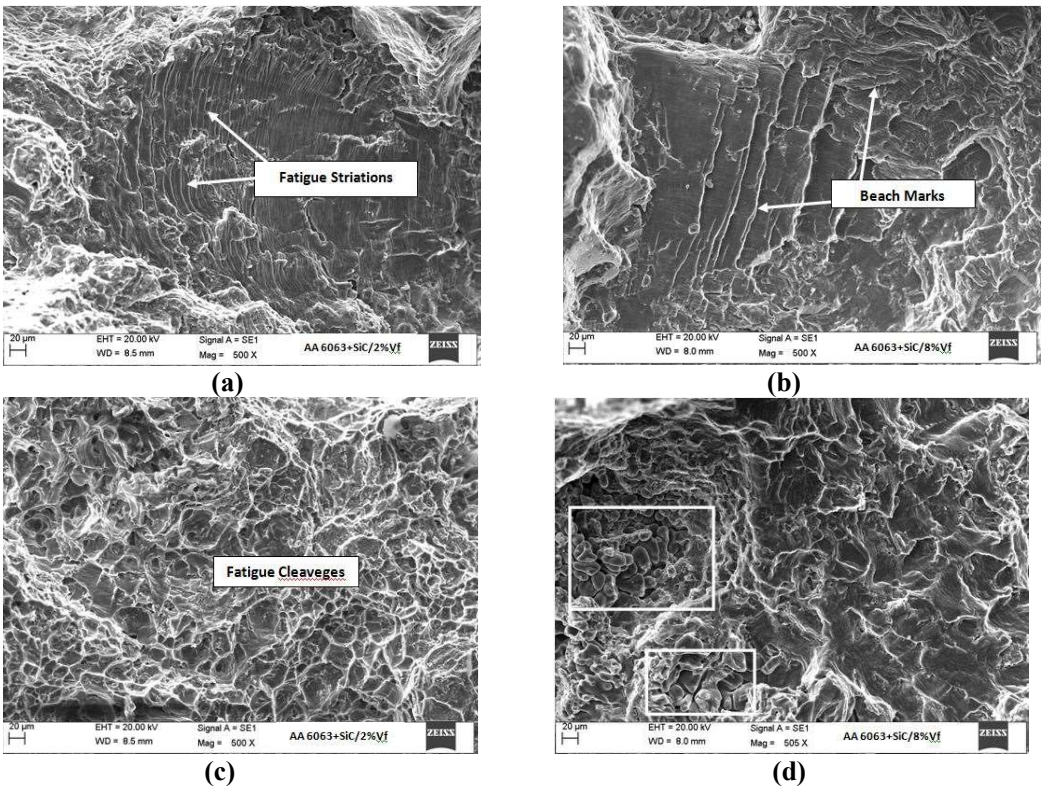

(a) **(b)**

(c) **(d)**

Fig. 36 SEM micrographs of MMC AA 6063/SiCp, (a) Fatigue striations at 2% V_f , (b) Beach marks of fatigue at 8% V_f, (c) Fatigue initiation region at 2% V_f, (d) Fast fracture region at 8% V_f

6. Conclusion

1. The experimental values of low cycle fatigue parameters viz. cyclic strain exponent and cyclic strength coefficient are in good agreement with that obtained by theoretical method.
2. The elastic and plastic strain on the surface of the specimen along the cross section of failure obtained by finite element analysis are in good agreement with the experimental values for all cases.
3. Strain hardening exponent decreases with volume fraction of reinforcement particle in MMC.
4. Transition fatigue life increases considerably with the increase in volume fraction of reinforcement particle.
5. Fatigue ductility exponent has increases with increase in volume fraction of reinforcement particle.
6. Fatigue ductility coefficient or cyclic plastic strain behavior is same to that of fatigue ductility exponent for volume fraction of MMC variation.
7. Fatigue strength exponent have almost constant with volume fraction of reinforcement particle in MMC.
8. Cyclic strength coefficient has decreasing tendency with increase in volume fraction of MMC.
9. Fatigue strength coefficient has decreasing with volume fraction of reinforcement particle in MMC.
10. Cyclic strain hardening exponent has decreases with increase in volume fraction of reinforcement particle in MMC.
11. Crystallite size decreases after increase in volume fraction of reinforcement particle in MMCs.
12. Observations of SEM pictures of fracture surfaces show low cycle fatigue features like crack initiation, ratchet marks, fatigue striations, fatigue cleavages, beach marks, progression marks and overload zones.
13. Optical micrograph of MMC clearly shows presence of reinforcement particles.
14. SEM pictures show overload zone, progression marks, striation marks for as received AA6063-T6, heat treated at different temperature, heat treated at different soaking time, MMC, simply support samples. For cantilever specimen the elongated overload zone proves presence of bending load. Progression and fatigue striation marks show cyclic loading and direction of propagation of crack.
15. Increasing SiC*p* volume percent resulted in increased fatigue life in the composites. The higher fatigue strength of the composites was due largely to lower total strain as a result of load transfer to the high modulus reinforcement.
16. The addition of SiC particles reduced the effective stress concentration on intermetallic inclusions in the matrix of the composite, increasing the fatigue life over the unreinforced alloy, where the inclusions had a higher stress concentration.
17. With increasing reinforcement volume fraction, yield strength and fatigue strength increased. With an increase in volume fraction, the number of sites for stress concentration increases, and the total amount of microplasticity also increases.

Acknowledgement

The author would like to acknowledge and convey their sincere gratitude to the Aeronautical Techniques Engineering Department, and Computer Techniques Engineering Department, Bilad Alrafidain University College, Iraq. Also would like to thank the Management and the Department of Mechanical Engineering IIT (BHU), India. The author would like to thank his parent for their inspiration, encouragement and excellent co-operation as well as financial support, and Dr Saadat Ali Rizvi, faculty member, University Polytechnic, Jamia Millia Islami,New Delhi, India.

References

Chawla, N., Jones, J. W., Andres, C., & Allison, J. E. (1998). Effect of SiC volume fraction and particle size on the fatigue resistance of a 2080 Al/SiC p composite. *Metallurgical and Materials Transactions A*, *29*(11), 2843-2854.

Ding, H. Z., Hartmann, O., Biermann, H., & Mughrabi, H. (2002). Modelling low-cycle fatigue life of particulate-reinforced metal-matrix composites. *Materials Science and Engineering: A*, *333*(1-2), 295-305.

Hadianfard, M. J., & Mai, Y. W. (2000). Low cycle fatigue behaviour of particulate reinforced metal matrix composites. *Journal of Materials Science*, *35*(7), 1715-1723.

Hall, J. N., Jones, J. W., & Sachdev, A. K. (1994). Particle size, volume fraction and matrix strength effects on fatigue behavior and particle fracture in 2124 aluminum-SiCp composites. *Materials Science and Engineering: A*, *183*(1-2), 69-80.

Koh, S. K., Oh, S. J., Li, C., & Ellyin, F. (1999). Low-cycle fatigue life of SiC-particulate-reinforced Al-Si cast alloy composites with tensile mean strain effects. *International Journal of Fatigue*, *21*(10), 1019-1032.

Knez, M., Glodež, S., Ružička, M., & Kramberger, J. (2010). A rotating bending approach for determination of low-cycle fatigue parameters. *International Journal of Fatigue*, *32*(10), 1724-1730.

Li, W., Chen, Z. H., Chen, D., Teng, J., & Fan, C. (2010). Low-cycle fatigue behavior of SiCp/Al–Si composites produced by spray deposition. *Materials Science and Engineering: A*, *527*(29-30), 7631-7637.

Megahed, M. M., Eleiche, A. M., & Abd-Allah, N. M. (1996). Low-cycle fatigue in rotating cantilever under bending I: Theoretical analysis. *International Journal of Fatigue*, *18*(6), 401-412.

Muratoğlu, M., Yilmaz, O., & Aksoy, M. (2006). Investigation on diffusion bonding characteristics of aluminum metal matrix composites (Al/SiCp) with pure aluminum for different heat treatments. *Journal of Materials Processing Technology*, *178*(1-3), 211-217.

Uygur, I., & KÜLEKCİ, M. K. (2002). Low Cycle Fatigue Properties of 2124/SiC_ {p} Al-Alloy Composites. *Turkish Journal of Engineering and Environmental Sciences*, *26*(3), 265-274.

Shang, J. K., & Ritchie, R. O. (1989). Crack bridging by uncracked ligaments during fatigue-crack growth in SiC-reinforced aluminum-alloy composites. *Metallurgical Transactions A*, *20*(5), 897-908.

Standarad, A. S. T. M. E606-04. (2005).Standard Practice for Strain-Controlled Fatigue Testing. ASTM International.

Srivatsan, T. S. (2002). An investigation of the cyclic fatigue and fracture behavior of aluminum alloy 7055. *Materials & design*, *23*(2), 141-151.